Progress In Electromagnetics Research C, Vol. 117, 55–72, 2021

Research on Shielding and Electromagnetic Exposure Safety of an Electric Vehicle Wireless Charging Coil

Wenting Mou[1] and Mai Lu[2, *]

Abstract—To address the problems of large volume, heavy weight, and inconvenient installation of the shield board of a wireless charging coil (WCC) installed on the body of an electric vehicle (EV), a new shielding method is proposed in this paper. From the perspective of engineering practice, according to the principle of passive shielding, and in line with the vertical direction of WCC with ferromagnetic material shielding, this novel shielding method involves only a low permeability metal shielding ring set around the transmitting coil in the horizontal direction. Using the finite element simulation software COMSOL Multiphysics, the EV model, the magnetic coupling resonance (MCR) WCC model, and the pedestrian body model at the observation point are designed. The influence of the metal shielding ring on the self-inductance and mutual inductance of WCC is calculated. The magnetic induction strength (B) and electric field strength (E) of pedestrian body at observation points before and after adding a metal shielding in the horizontal direction are evaluated, and the electromagnetic exposure safety of a pedestrian body in this electromagnetic environment is analyzed. Compared with the shielding method of only adding ferromagnetic material in the vertical direction and after using new shielding, the maximum B of a human trunk is reduced by 43%, the maximum E reduced by 44%, the maximum B of human head reduced by 44%, and the maximum E reduced by 39%. After adding the metal shielding ring, the maximum B and E of human trunk decreased from 8.56×10^{-1} times and 2.28×10^{-1} times of the International Commission on Non-Ionizing Radiation Protection (ICNIRP) exposure limit to 4.89×10^{-1} times and 1.27×10^{-1} times, respectively, and the maximum B and E of human head decreased from 1.62×10^{-3} times and 8.58×10^{-4} times of the ICNIRP exposure limit to 9.18×10^{-4} and 5.25×10^{-4} times, respectively. The simulation results show that the new shielding method can significantly reduce the electromagnetic radiation of the pedestrian's trunk and head central nervous system (CNS) at the observation point. The effectiveness of the shielding method is proven, and this work provides a certain guidance for the engineering design of WCCs.

1. INTRODUCTION

Wireless power transfer (WPT) electric vehicles (EVs) can promote energy conservation and emission reduction. However, the WPT system of an EV runs in an open environment, and its emission power can be as high as tens of kilowatts. When that energy is transmitted through the air, considerable electromagnetic emissions would be generated. As the main electromagnetic leakage source of EVs, the WPT system will pose a health threat to the human body exposed to time-varying electromagnetic fields. Therefore, the magnetic flux leakage shielding and electromagnetic exposure safety of WPT EVs have attracted much attention [1, 2].

Received 27 July 2021, Accepted 8 December 2021, Scheduled 19 December 2021

* Corresponding author: Mai Lu (mai.lu@hotmail.com).

[1] Institute of Railway Technology, Lanzhou Jiaotong University, Anning District, Lanzhou 730070, China. [2] Key Laboratory of Opto-Electranic Technology and Intelligent Control, Ministry of Education, Lanzhou Jiaotong University, Anning District, Lanzhou 730070, China.

Two methods are predominantly adopted for passive shielding from the magnetic flux leakage of WPT EVs: the use of ferromagnetic materials with high permeability to provide a new conduction path for the magnetic flux [3] and of good conductors with low resistivity to produce a magnetic field opposite to the magnetic flux leakage so as to play a shielding role. Those two shielding methods are compared in [4], in which the magnetic field leakage can be reduced by using ferromagnetic materials; the self-inductance and mutual inductance of the coil can be increased; the coupling of the coil can be enhanced; and the system efficiency can be improved, but the shielding effect is limited. Although a low permeability metal shielding can effectively shield from magnetic field leakage, it will lead to the decrease of system efficiency; accordingly, some scholars have adopted the shielding structure of ferromagnetic materials combined with low permeability metals [5, 6]. Ferromagnetic materials have a certain shielding effect on the coil electromagnetic field, and combined with non-ferromagnetic shielding materials, the vertical leakage field of the shielding body is suppressed, but the horizontal leakage field does not decrease. In terms of the electromagnetic shielding of the WCC, the addition of ferromagnetic material on the outside of WCC and the overall aluminum shielding plate on the outside of the receiving coil and transmitting coil is the prevalent approach. However, the electromagnetic shielding function of the body and chassis metal of the EV means that adding the overall aluminum shielding plate on the receiving side will not only waste materials, but also increase the EV weight and affect the driving range. To overcome the above defects, Reference [7] analyzes the influence of shielding on the transfer characteristics of WPT system by using whole plate shielding and circular rings. To reduce the shielding loss and ensure the transmission efficiency, References [8, 9] introduce a litzshield method to attenuate the magnetic field through uniform distribution shield current and proves the shielding effect of the shorted litz shield. The shielding effect of a car body material itself is not considered in the above shielding methods, and the metal shielding is no longer needed under the transmitting coil installed on the ground. Therefore, the practicability is not very strong. In application, the electromagnetic environment in a WPT EV is relatively safe because of the protection of car body materials. For the safety of the electromagnetic exposure of pedestrians near WPT EVs, reducing the horizontal magnetic leakage field of a WCC is worthy of consideration.

In terms of electromagnetic exposure safety, Reference [10] evaluates the electromagnetic measurement of a WPT EV under different exposure conditions, but only the WCC is considered in the analysis, and the car body is not considered. The compliance of the electromagnetic exposure limits of a wireless charging system (WCS) to the human body is verified in [11], wherein a steel plate is used to replace the car body, but the model is too simplified, and the practical significance is not very strong. In [12], the in-situ electric field of human body models with different postures under wireless charging with a resonant frequency of 85 kHz and a charging power of 7 kW is studied. Reference [13] examines the influence of different coil designs on the internal electric field of the fetus and its mother. Reference [14] investigates the RF energy absorption of human models with different implants in the electromagnetic exposure environment of wireless charging. Although the car body is considered in the above literature, the material of the car body is not considered. In [15], the electromagnetic exposure of the carbon fiber EV with an output power of 7.7 kW is explored under the most unfavorable condition of misalignment of the transmitting and receiving coils. A small part of the driver's foot exceeds the ICNIRP limit. The car body and car body materials are considered in the analysis, but there is no further explanation on how to reduce the electromagnetic radiation of human feet. The shielding effect of different car body materials on WPT electromagnetic metrology is evaluated in [16]. Reference [17] evaluates the influence of loudspeakers on the in-situ electric field of a driver's body in the magnetic field of the EV radio energy transmission system, and the results show that the distribution of the magnetic field produced by the WPT changes obviously around the loudspeaker, with obvious discontinuity and local enhancement. However, in [16] and [17], only the drivers and passengers in the car are considered in the analysis, and the pedestrian outside the car is overlooked.

In summary, designing a simple and practical shielding method is vital to reduce the leakage magnetic field in the horizontal direction of a WCC and reduce the electromagnetic radiation to the pedestrians outside an EV after selecting the general automobile model and fully considering the shielding effect of the car body material.

From the point of view of engineering practice, this study proposes a new shielding method of adding ferromagnetic material in the vertical direction of a WCC and only setting a non-ferromagnetic metal

shielding ring around the transmitting coil in the horizontal direction. The influence of metal shielding rings with different materials in the horizontal direction of the self-inductance and mutual inductance of WCC coils is analyzed. Through the establishment of an accurate electromagnetic environment simulation model of EV, the electromagnetic radiation changes of pedestrians at the observation point before and after the WCC horizontal direction with a shielding ring are compared. The safety of the human body in the electromagnetic environment is evaluated, and the effectiveness of the new shielding method is verified.

2. ELECTROMAGNETIC ENVIRONMENT SIMULATION MODEL OF AN EVWCS

The field circuit coupling method based on circuit theory and an accurate three-dimensional finite element model is adopted in this work. As the electromagnetic wave of the MCR WCS is larger than the transmission distance, the magnetic quasi-static method is utilized to analyze the electromagnetic environment of the WCS. The electromagnetic environment simulation model established in COMSOL Multiphysics 5.5 is shown in Fig. 1, and the frequency domain is analyzed. The WCC is placed in the middle of the EV chassis. Given the symmetrical effect of the electromagnetic field around the WCC, only one side of the car door is selected as the observation point. The electromagnetic radiation test point should be the closest point of the exposed area outside the EV, but the position of the test point will change with the EV type. According to the recommendations of Society of Automotive Engineers (SAE) J2954, the vertical distance between the center of the toes of the human feet and the center of the WCC is 800 mm [18]. The distance between the human head and the center of WCC is 1,000 mm

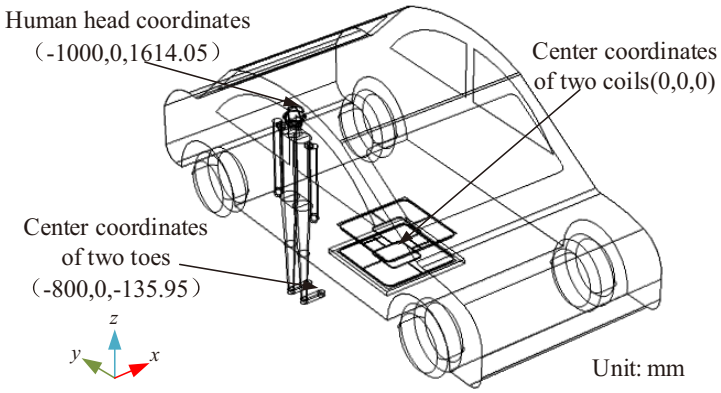

Figure 1. Relative position of the human body, EV, and WCC.

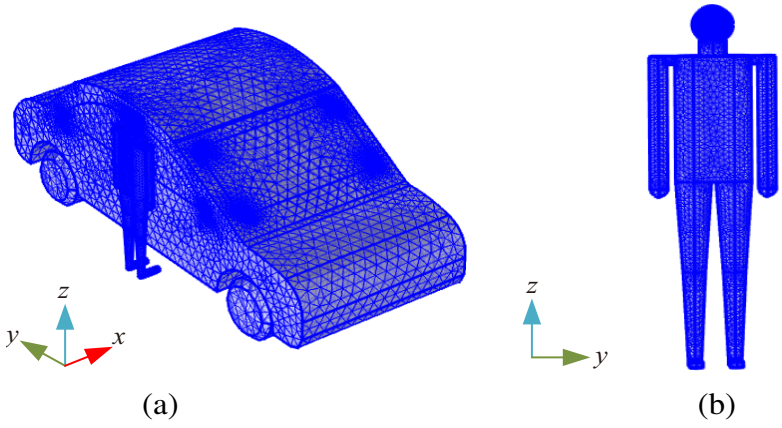

Figure 2. Finite element discrete model. (a) Global finite element model. (b) Finite element model of the human body.

in the X direction, 0 mm in the Y direction, and 1,614.05 mm in the Z direction. After the assignment of a car body and other materials, the adjusted circuit parameters are substituted; the air domain and infinite element domain are established outside the overall model; the absorbing boundary conditions are set; and the finite element discrete model is obtained as shown in Fig. 2. The entire model is divided into 1,155,563 units, including 365,722 tetrahedral units, 1,242 prismatic units, 62,325 triangular units, 192 quadrilateral units, 6,303 edge units, and 452 vertex units. Since this study focuses on the CNS of the human body, the human head is divided by ultra-fine mesh; the maximum unit of the human head is 8 mm; and the minimum unit is 1.2 mm, including 48,471 units for the head model and 74,852 units for the trunk model.

2.1. WCC Model with a New Shielding

At present, the two main application standards of WPT in an EV include the 61980 standard adopted by the International Electrotechnical Commission (IEC) and the J2954 standard adopted by the SAE [19]. The two standards mainly specify the transmission power and working frequency of a WPT system. The 3 kW to 11 kW WCS designed in the SAE J2954 operates in the frequency band of 79 kHz to 90 kHz. To better observe the radiation effect, this work selects the WPT3 11 kW WCC working at 85 kHz for research.

The MCR WCC model with new shielding proposed in this work is shown in Fig. 3. Given the electromagnetic shielding effect of the car body material itself, the driver and passengers are exposed to very little electromagnetic radiation inside the car. Therefore, this study considered the use of ferromagnetic materials in the vertical direction of the WCC to increase the coupling of the coil and of non-ferromagnetic metal shielding ring in the horizontal direction of the WCC to reduce the horizontal electromagnetic exposure. The transmitting and receiving coils of wireless charging consist of 10 turns of copper wires. The ferromagnetic material outside the vertical direction of the coil is a 3 mm-thick ferrite

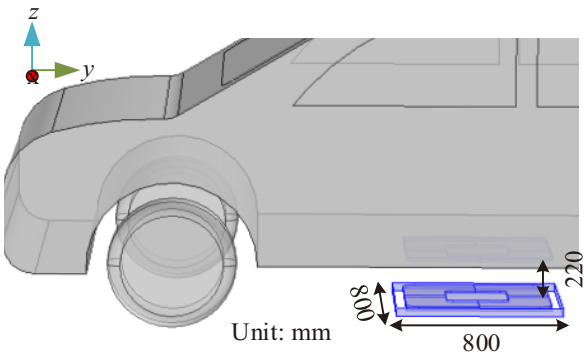

Figure 3. WCC with new shielding.

Table 1. Model parameters of WCC.

Parameter	Numerical value
Dimensions of ferrite plate (length × width × height)/(mm × mm × mm)	700 × 700 × 3
Peripheral dimension of shielding ring (length × width)/(mm × mm)	800 × 800
Distance between two coils/mm	220
Coil turns/n	10
Resonant frequency/kHz	85
Effective value of transmitting power/kW	11.02

plate, and its relative permeability is 2,300. The transmitting coil is on the ground, and the receiving coil is under the chassis of the car. The transmission distance between the transmitting and receiving coils is 220 mm. To achieve a better magnetic shielding effect without affecting the transmission efficiency of the system, the horizontal metal shielding ring must be placed far away from the transmitting coil. Through simulation tests, a square metal shielding ring is finally set at 50 mm outside the WCC transmitting coil. The metal used for the shielding ring is 1 mm thick and 40 mm high, and the size of the enclosed square shielding ring is 800 mm × 800 mm. In the actual installation, the metal can be inserted into the ground around the transmitting coil, is easy to install, and also saves materials. The model parameters of the MCR WCC are shown in Table 1.

2.2. Car Body Model

When the WCC resonates, energy is transferred through the electromagnetic field of the space. The change of the magnetic field between the two coils will affect circuit impedance, and the material of the car body and chassis can affect the coupling of the two coils. In the selection of car body materials, aluminum alloy, low carbon steel, and carbon fiber reinforced plastics (CFRP) are considered. To compare the B at the observation point under the influence of three kinds of car body materials, a stub line with a length of 1 mm is made between 799 mm and 800 mm from the center of the WCC. The relative position of the stub line and the WCC is shown in Fig. 4. The B at the stub line under the influence of different car body materials is calculated by simulation as shown in Fig. 5. Although the shielding effect of the aluminum alloy car body is optimal for the electromagnetic safety of passengers in the EV, the B at the observation point is the highest when the car body is aluminum alloy because the selected observation point is not within the protective range of the car body. To select the most unfavorable radiation conditions for comparing the shielding effect of the metal shielding ring, an aluminum alloy car body is selected as the research object. The size of the car body is 4318 mm × 1783 mm × 1730 mm (length × width × height), is similar to the commercially available vehicle, and can provide a good reference. Detailed dielectric parameters of the EV model are shown in Table 2. The dielectric parameters of aluminum alloy car body are from COMSOL Multiphysics material library, and the dielectric parameters of window glass are from Reference [20].

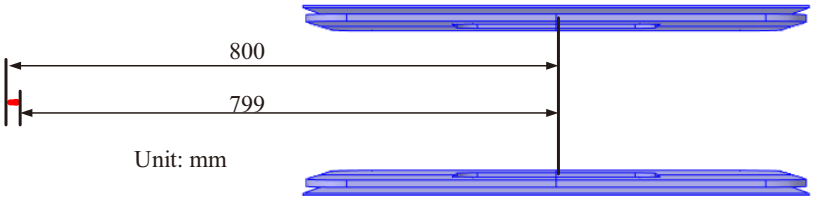

Figure 4. Stub line at observation point.

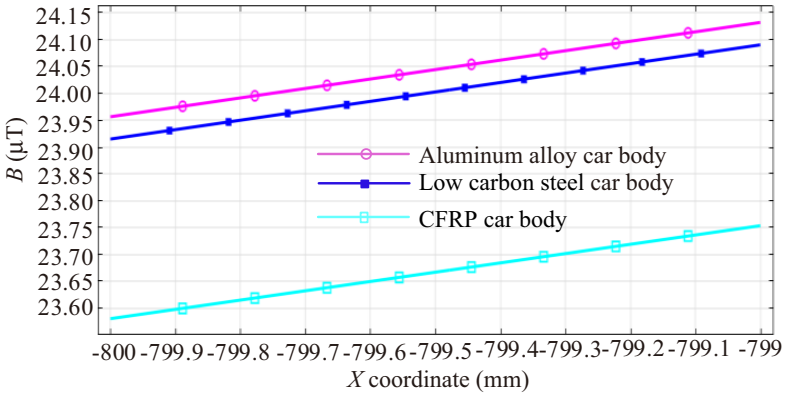

Figure 5. B at the stub line.

Table 2. Dielectric parameters of the EV.

Body and window of the EV	Relative permittivity	Conductivity/(S/m)	Relative permeability μ_r
Aluminum alloy car body	1.00	2.33×10^7	1.00
Window glass	5.50	1.00	1.00

2.3. Human Body Model

As the electrical and magnetic field strengths of the human body cannot be evaluated by measurement, numerical simulation is widely used to ascertain the electromagnetic field distribution of the human tissue [21, 22]. The human body consists of a head model and a trunk model as shown in Fig. 6. The head model is divided into the three layers of scalp, skull, and brain, with radii of 92 mm, 85 mm, and 80 mm, respectively [23]. The height of the human body model is 1,750 mm. For the research on the electromagnetic parameters of human tissues, it is assumed that human tissues are composed of evenly distributed media. Internationally, for the selection of dielectric parameters of human tissues, 4-Cole-Cole model is generally used to calculate the electromagnetic parameters of human tissues. The 4-Cole-Cole model is that Gabriel extracts different tissues of human body, obtains the conductivity and relative dielectric constant at different frequencies, and creates the 4-Cole-Cole model to simulate the electromagnetic parameters of human tissue in the frequency range of 10 Hz to 20 GHz. The relative permittivity and conductivity of the human tissue at 85 kHz are calculated by a 4-cole-cole model [24]. The relative permittivity and conductivity of human tissues at 85 kHz are shown in Table 3. The parameters of the trunk tissue include the average values of skin, blood, muscle, and bone [25, 26].

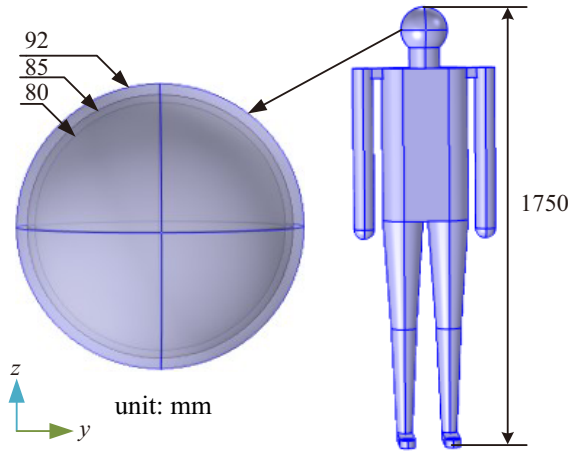

Figure 6. The human body model.

Table 3. Permittivity and conductivity of human tissue at 85 kHz.

Human model tissue	Relative permittivity	Conductivity/(S/m)
Scalp	9.06×10^3	2.80×10^{-2}
Skull	2.85×10^2	3.59×10^{-2}
Brain	2.04×10^3	7.38×10^{-1}
Trunk	5.75×10^3	2.81×10^{-1}

3. ANALYSIS OF THE SIMULATION RESULTS

3.1. Influence of the Horizontal Non-Ferromagnetic Metal Shielding Ring on the Self-Induction and Mutual Induction of the WCC

As the new shielding in this study focuses on reducing the horizontal electromagnetic exposure of the WCC, and the reduction of horizontal electromagnetic exposure mainly depends on the eddy shielding effect caused by adding a low permeability metal in the horizontal direction of the WCC, the influence of the horizontal metal shielding coil on the self-induction and mutual induction of the WCC is analyzed. In electromagnetic field engineering, electromagnetic shielding is used to weaken the electromagnetic field generated by the exposed source in a certain area of space (excluding the exposed source). Three metals (aluminum, copper, and steel) are selected as shielding ring materials for comparative analysis. The dielectric parameters of the three metal materials are shown in Table 4. The dielectric parameters in Table 4 are from COMSOL Multiphysics material library.

Table 4. Dielectric parameters of the metal shielding ring.

Parameter	Relative permittivity	Conductivity/(S/m)	Relative permeability μ_r
Aluminum	1	2.33×10^7	1
Copper	1	6.00×10^7	1
Steel	1	4.03×10^6	50

Adding the metal shielding ring will have a certain impact on the self-inductance, mutual inductance, and coupling coefficient of the WCC. The parameters calculated by simulation are shown in Table 5.

Table 5. Influence of the horizontal metal shielding ring on the self-inductance and mutual inductance of the coil.

Metal shielding ring	Self inductance of transmitting coil L_1 (μH)	Self inductance of receiving coil L_2 (μH)	Mutual inductance M (μH)	Coupling coefficient K	Transmission efficiency
No shielding	98.462	94.127	27.055	0.275	95.53%
Aluminum	91.315	92.622	23.779	0.260	95.58%
Copper	91.305	92.620	23.776	0.260	95.72%
Steel	91.375	92.633	23.804	0.261	94.85%

Table 5 indicates that the metal shielding rings made of aluminum, copper, and steel have very similar influences on the self-inductance and mutual inductance of the WCC. The addition of copper, aluminum, and steel metal shielding rings reduces the self-inductance and mutual inductance of the WCC, thereby causing a decrease in the coupling coefficient of the WCC. The self-inductance of the transmitting coil is reduced by approximately 7%, and that of the receiving coil is reduced by approximately 2%. The coupling coefficient is reduced by approximately 5%, but the transmission efficiency is basically unchanged.

3.2. Effect of the Horizontal Metal Shielding Ring on B in Space

To analyze the influence of the metal shielding ring on the horizontal space B, the ZX section is taken at the space center $y = 0$, and the distribution of B at the cross section is analyzed under the shielding of different metal shielding rings. The B distribution is shown in Fig. 7. In Fig. 7(a), the material of the metal shielding ring is equivalent to air to achieve the effect of the absence of a shielding ring, and the maximum B is concentrated around the WCC, and fast attenuation around. As the shielding ring

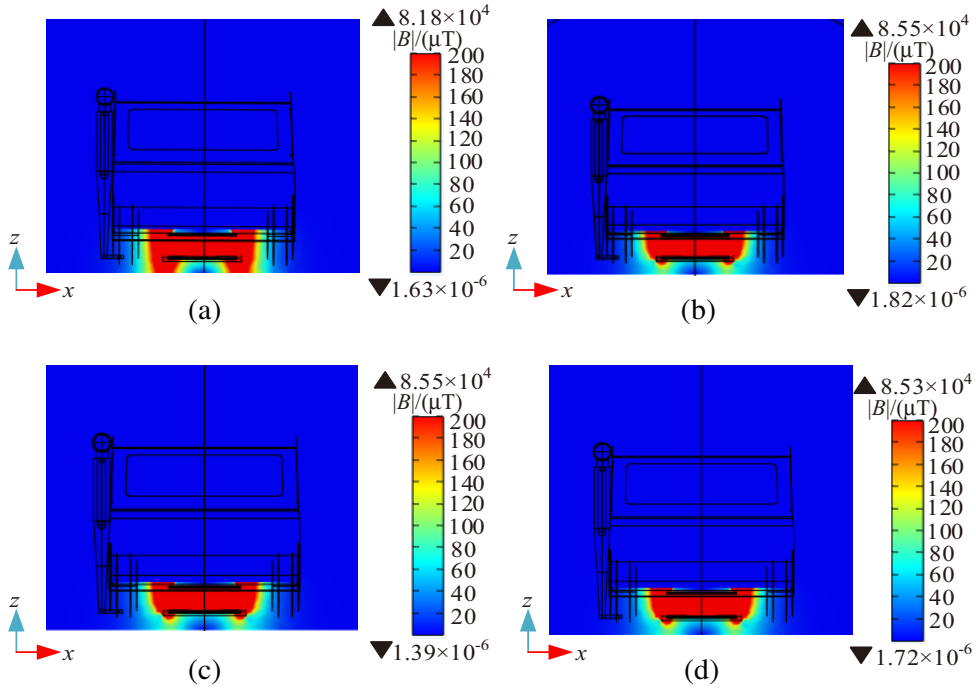

Figure 7. Distribution of B in space section. (a) No shielding ring in horizontal direction. (b) Aluminum shielding ring in horizontal direction. (c) Copper shielding ring in horizontal direction. (d) Steel shielding ring in horizontal direction.

material is set as air, B is uniformly distributed in Fig. 7(a), and no truncation and suppression of the shielding ring occur on the magnetic field. In Figs. 7(b), (c), and (d), the maximum value of B is also concentrated around the transmitting and receiving coils, and fast attenuation around. Compared with Fig. 7(a) without the shielding ring, the aluminum, copper, and steel shielding rings have significant suppression effects on the horizontal magnetic leakage field, because when the metal shielding ring is in the high frequency alternating electromagnetic field, it can produce the induced current. The induced current is closed in the metal shielding ring and forms the eddy current. The electromagnetic field generated by the eddy current resists the original electromagnetic field and weakens the magnetic field on the metal shielding ring until the high frequency alternating magnetic field cannot pass through the metal shielding ring.

3.3. Influence of the WCC Horizontal Metal Shielding Ring on Spatial E

To observe the influence of metal shielding rings with different materials on the E in a horizontal direction, the ZX section is taken at the space center $y = 0$ to analyze the E distribution of the WCC with different shielding materials in the horizontal direction. The E distribution is shown in Fig. 8. In Fig. 8(a), the material of the WCC horizontal metal shielding ring is set as air to achieve the effect of the absence of a shielding ring. The maximum E is concentrated around the WCC and fast attenuation around. As the car body material is set as air, E is evenly distributed in Fig. 8(a), and no suppression phenomenon of the shielding ring occurs on the horizontal E. In Figs. 8(b), (c), and (d), the maximum E is also concentrated around the transmitting and receiving coils, and fast attenuation around. Compared with Fig. 8(a) without the shielding ring, the aluminum, copper, and steel shielding rings have significant suppression effect on the horizontal leakage electric field.

According to the above analysis, the shielding effects of copper, aluminum, and steel shielding rings on the magnetic and electric fields of the space are similar. The effects on the self-inductance and mutual inductance of the coil are almost the same. The shielding ring material in this work is considered to be installed under the ground, and copper is superior to aluminum and steel in terms of heat dissipation

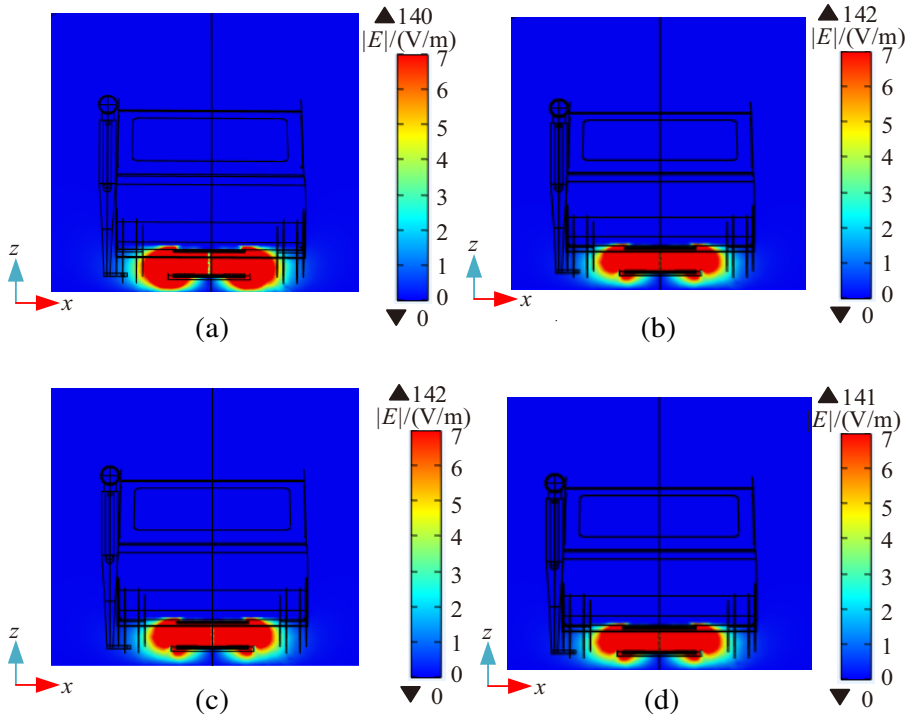

Figure 8. Distribution of E in the space section. (a) No shielding ring in horizontal direction. (b) Aluminum shielding ring in horizontal direction. (c) Copper shielding ring in horizontal direction. (d) Steel shielding ring in horizontal direction.

and corrosion resistance. Thus, copper is selected as the material of the WCC horizontal metal shielding ring.

3.4. Comparison of the Human Body Radiation at the Observation Point

Shielding effect is usually expressed by shielding effectiveness (SE) [27–29], but it calculates a point in space, not the human body. The permeability of human tissue is the same as that of air, so the magnetic field inside the tissue is the same as that outside the tissue, and the human body will not noticeably interfere with the magnetic field. However, in terms of the electric field, the human body will change the low-frequency electric field in the environment. To accurately evaluate the electromagnetic exposure of the human body in this electromagnetic environment, this work directly uses the human body as the observation point to evaluate the shielding effect of a new shielding method and analyzes the electromagnetic exposure safety of the WCC.

The distribution of B of the human body in this electromagnetic environment is shown in Fig. 9. The toes are the closest to the WCC, so the maximum B of the human body under different shielding conditions occurs at the toes, followed by the lower leg. When no metal shielding occurs in the horizontal direction of the WCC, the maximum value of the human B is 2.31×10^1 μT. After adding the copper shielding ring, the maximum B of the human body is reduced to 1.32×10^1 μT, a figure which is approximately 57% of that without the shielding ring. The comparison of the B of the human body shows that the WCC horizontal copper shielding ring plays a satisfactory role in reducing the B of the human body.

The distribution of E of the human body in the electromagnetic environment is shown in Fig. 10. The toes are the closest to the WCC, so the maximum E of the human body under different shielding conditions occurs at the toes, followed by the lower leg. When no metal shielding occurs in the horizontal direction of the WCC, the maximum E of the human body is 2.63 V/m. After adding the copper shielding ring, the maximum E of the human body is reduced to 1.47 V/m or approximately 56% of

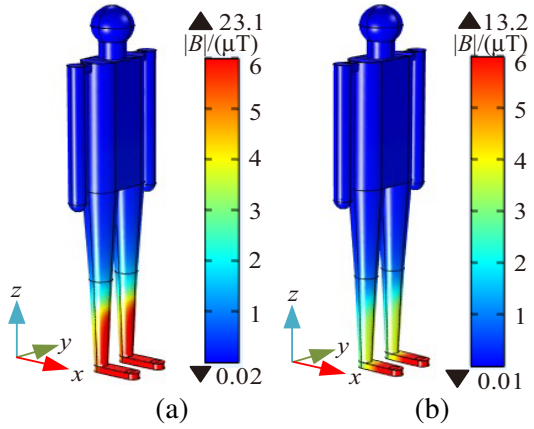

Figure 9. Distribution of the B of the human body. (a) No shielding ring in horizontal direction. (b) Copper shielding ring in horizontal direction.

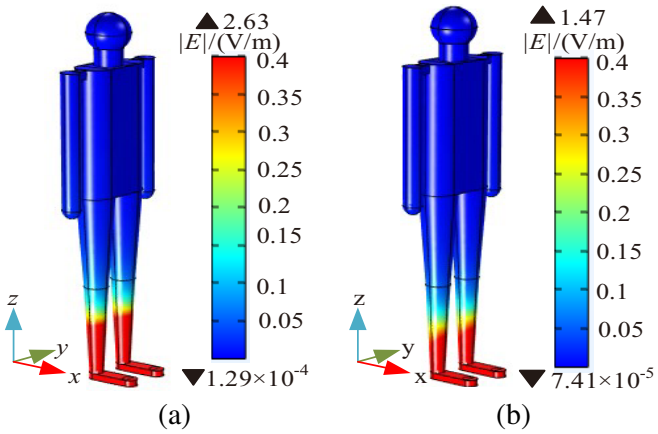

Figure 10. E distribution on the human body. (a) No shielding ring in horizontal direction. (b) Copper shielding ring in horizontal direction.

that without shielding ring. The WCC horizontal copper shielding ring plays a good role in reducing the E of the human body.

Under repeated low intensity electromagnetic exposure, the CNS of the human body may exhibit the neurasthenia phenomenon, which has an impact on health [30]. To analyze the protective effect of the horizontal copper shielding ring on the electromagnetic exposure of the CNS of the human head, a three-dimensional transversal line is made on the head of the pedestrian as shown in Fig. 11. The starting point of the three-dimensional transversal line of the human head is -1 mm, -0.092 mm, and 1.52205 mm, and the ending point is -1 mm, 0.092 mm, and 1.52205 mm. The B and E at the three-dimensional transversal line of the human head under this shielding condition are analyzed.

In the case without shielding and copper shielding in the horizontal direction of the WCC, the B and E at the three-dimensional transversal line of the human head are shown in Fig. 12. Fig. 12(a) shows the B curve of the three-dimensional transversal line of the human head. Fig. 12(b) shows the E curve of the three-dimensional transversal line of the human head. After the copper shielding ring is installed, the B at the transversal line of the human head decreases from approximately 0.03 μT to 0.017 μT. The maximum E at the transversal line of the human head decreases from approximately 0.0085 V/m to 0.005 V/m. Therefore, the introduction of the WCC horizontal copper shielding ring can significantly reduce the B and E of the human head CNS.

To further observe the effect of the horizontal copper shielding ring of the WCC on the electromagnetic exposure of human head CNS, the radiation received by human CNS with or without

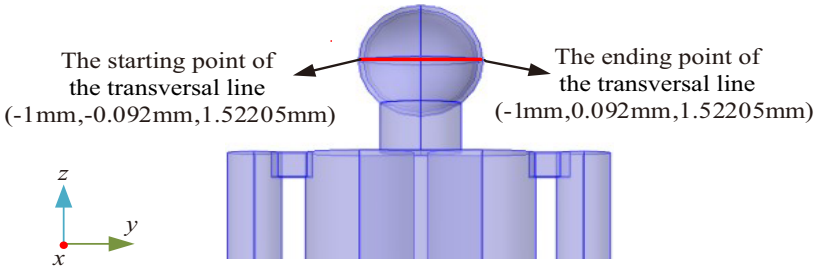

Figure 11. Three-dimensional transversal line of the human head.

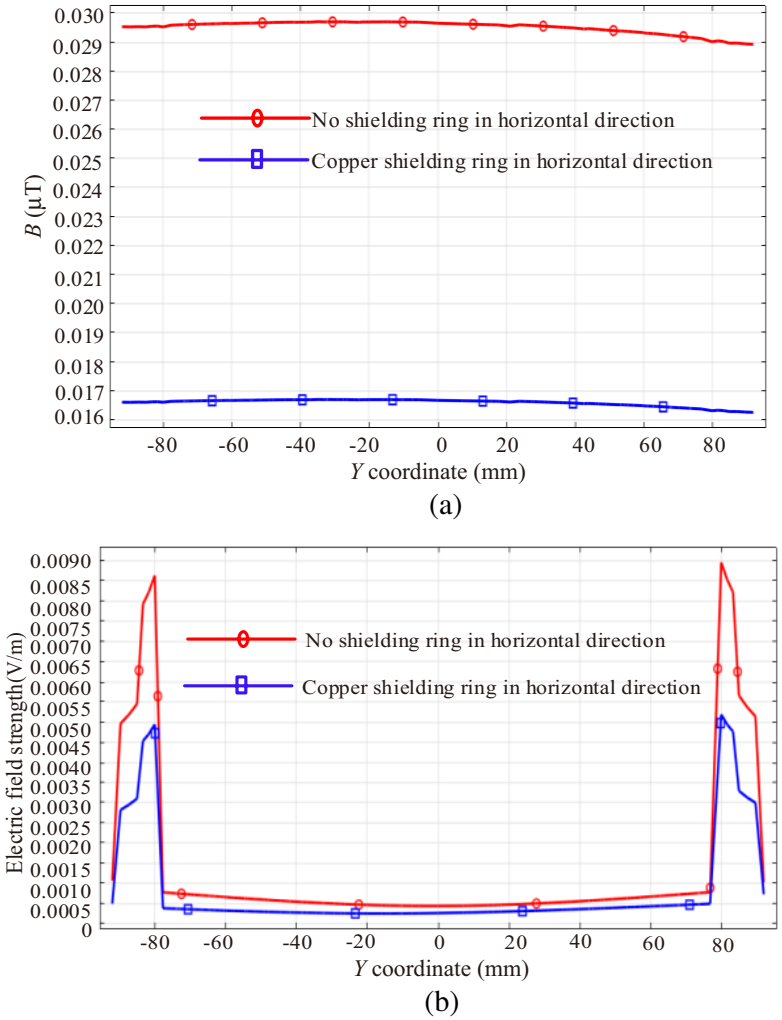

Figure 12. B and$E$ at the three-dimensional transversal line of the human head. (a) B at the three-dimensional transversal of the human head. (b) E at the three-dimensional transversal of the human head.

horizontal copper shielding ring of WCC is compared. The cross and longitudinal sections of the center of the human head are respectively made, as shown in Fig. 13, to analyze the distributions of B and E on the human head.

The B distribution of the human head is shown in Fig. 14. Fig. 14(a) shows the B distribution of the human head in the horizontal direction of the WCC without shielding. Fig. 14(b) presents the B

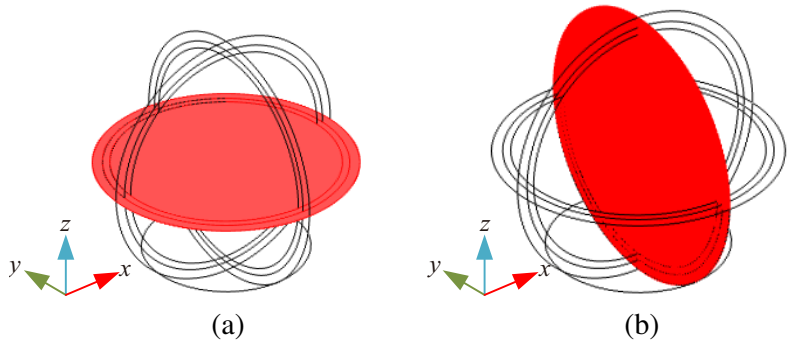

Figure 13. Head sections of the human model. (a) Head cross section. (b) Head longitudinal section.

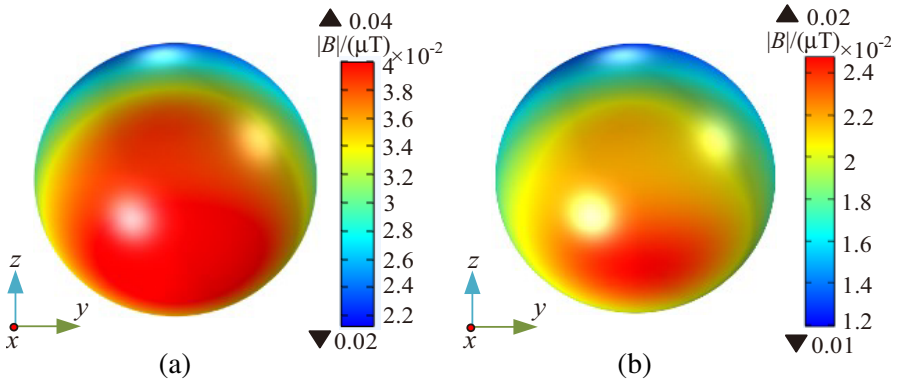

Figure 14. Distribution of the B of the human head. (a) No shielding in horizontal direction. (b) Copper shielding in horizontal direction.

distribution of the human head in the horizontal direction of the WCC with copper shielding. As can be seen in Fig. 14, the maximum and minimum B values of the human head are 0.04 μT and 0.02 μT when no shielding is present in the horizontal direction of the WCC. The maximum and minimum B values of the human head are 0.02 μT and 0.01 μT when a copper shielding ring is present in the horizontal direction of the WCC. The B of the human head decreases by 50% with the addition of the WCC horizontal copper shielding ring.

The distribution of B at the cross and longitudinal sections of the human head is shown in Fig. 15. B is evenly distributed in the head of the human body. The closer the human head is to the WCC, the greater the maximum value of B is. Thus, the value of B is related to the distance from the radiation source, and this value decreases with the increase of the distance. When the horizontal direction of the WCC is unshielded, the maximum B at the cross section of the human head is 0.04 μT. The maximum B at the cross section of the head is 0.02 μT with a copper shielding ring. Compared with the calculation results, the maximum B at the cross section of the human head can be reduced by 50% with the addition of the WCC horizontal copper shielding ring. The maximum B at the longitudinal section of the human head is 0.03 μT without shielding in the horizontal direction of the WCC, and the maximum B at the longitudinal section of the human head is 0.02 μT with a copper shielding ring. The calculation results indicate that the maximum B at the longitudinal section of the human head is reduced by 33% with the addition of the WCC copper shielding ring in the horizontal direction.

The E distribution on human head is shown in Fig. 16. Fig. 16(a) shows the E distribution of the human head when the WCC is horizontally unshielded. Fig. 16(b) shows the distribution of E of the human head when the WCC is horizontally shielded by copper. When no shielding is present in the horizontal direction, the maximum and minimum E of the human head are 9.87×10^{-3} V/m and 1.27×10^{-4} V/m. When the horizontal direction of the WCC is shielded, the maximum E of the human head is 6.04×10^{-3} V/m, and the minimum is 7.37×10^{-5} V/m. The copper shielding in the horizontal

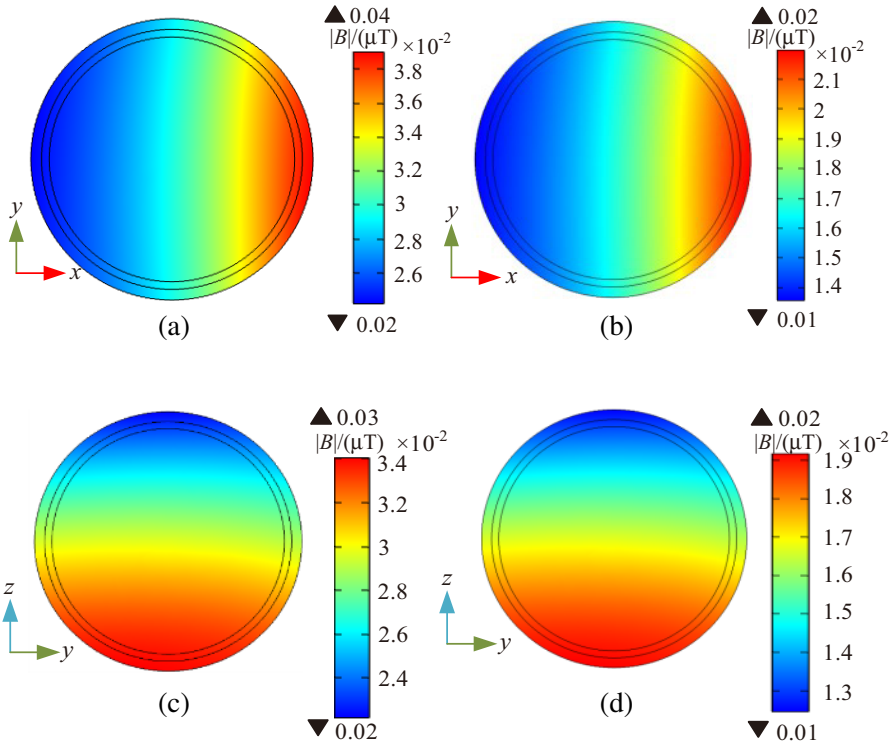

Figure 15. Distribution of the B at the cross and longitudinal sections of the human head. (a) Cross section (no shielding in horizontal direction). (b) Cross section (copper shielding in horizontal direction). (c) Longitudinal section (no shielding in horizontal direction). (d) Longitudinal section (copper shielding in horizontal direction).

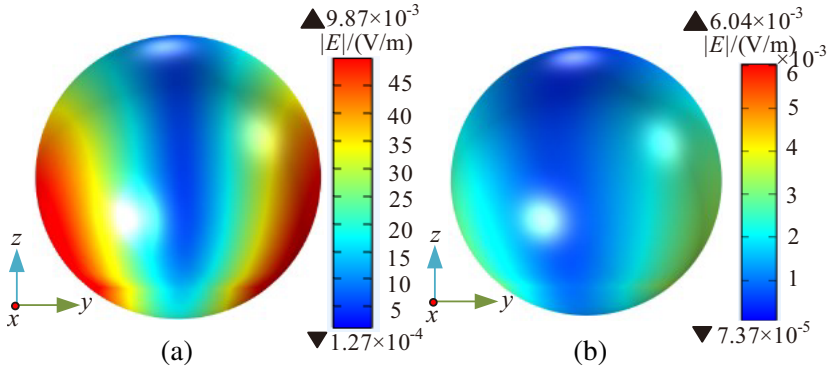

Figure 16. E distribution on the human head. (a) No shielding in horizontal direction. (b) Copper shielding in horizontal direction.

direction of the WCC reduced the E by 39% at the maximum and 42% at the minimum. Thus, the shielding ring plays a good role in reducing the E of the human head.

Figure 17 shows the E distribution of the human head at the cross and longitudinal sections. As can be seen from Figs. 17(a) and (b), when the horizontal direction of WCC is unshielded, the maximum E at the cross section of the human head is 9.08×10^{-3} V/m. In the case of copper shielding, the maximum E of the cross section of the human head is 5.62×10^{-3} V/m. The maximum E at the cross section of the head is reduced by 38% with the addition of the shielding ring. As can be seen from Fig. 17(c), when the horizontal direction of the WCC is unshielded, the maximum E at the longitudinal section of the human head is 9.7×10^{-3} V/m. In the case of copper shielding, the maximum E of the longitudinal

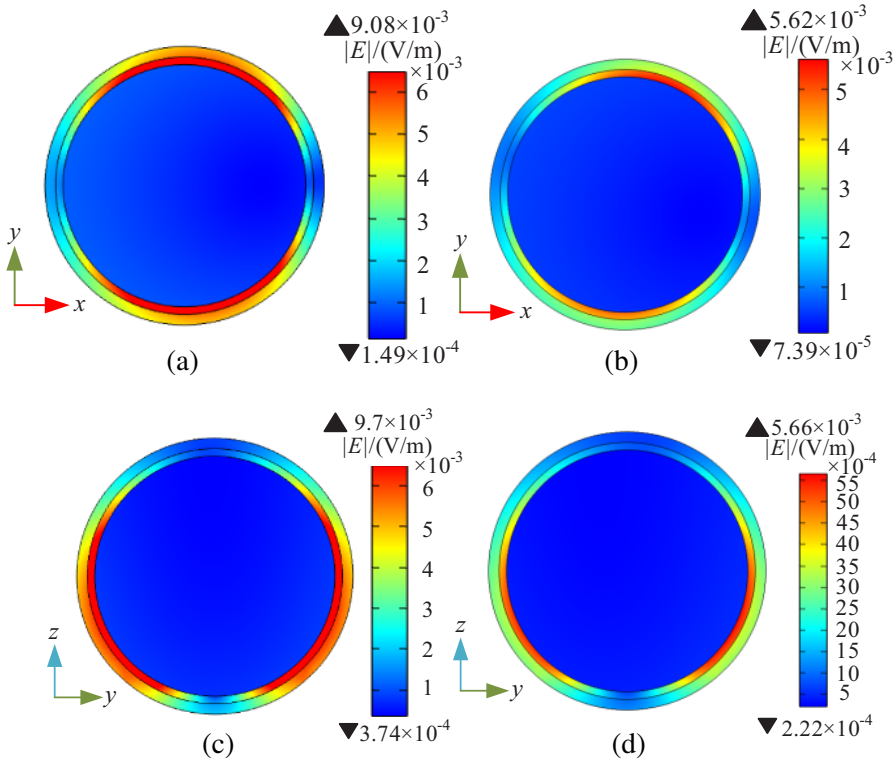

Figure 17. Distribution of E in cross and longitudinal sections of the human head. (a) Cross section (no shielding in horizontal direction). (b) Cross section (copper shielding in horizontal direction). (c) Longitudinal section (no shielding in horizontal direction). (d) Longitudinal section (copper shielding in horizontal direction).

section of the human head is 5.66×10^{-3} V/m. The maximum E at the longitudinal section is reduced by 42% with the addition of the shielding ring. E is not evenly distributed in the head of the human body, and the low frequency electric field changes obviously after entering the human head. E is strong in both ears of the human head. The maximum E of the entire head is concentrated in the skull layer, followed by the scalp layer. The E penetrating into the brain is very small.

3.5. Comparison of Limit Compliance

The ICNIRP guidelines are the most recognized nonionizing radiation EMC criterion at present and play a very good role in the EMC design of the MCR WCS of EVs [31, 32]. The said guidelines set a public exposure reference limit of 2.70×10^{1} μT for B (μT) and 1.15×10^{1} V/m for E (V/m) at a frequency of 85 kHz. The simulation values are compared with the public exposure limits in ICNIRP, and the relevant limits are shown in Tables 6 and 7.

As can be seen from Table 6, the maximum B of the human head is smaller than that of the trunk. For the human head, the maximum B of the scalp is greater than that of the skull and brain, and the maximum B of the brain is smaller than that of the scalp and skull. When no shielding ring is present in the horizontal direction of the WCC, the maximum B values of the human trunk and head are greater than that with a copper shielding ring. With the addition of the copper shielding ring in the horizontal direction of the WCC, the maximum B of the human trunk and head decreased to 5.7×10^{-1} times and 5.6×10^{-1} times of that without the shielding ring in the horizontal direction of the WCC.

As can be seen from Table 7, the maximum E of the head is smaller than that of the trunk. For the human head, the maximum E of the skull is greater than that of the scalp and brain, and the maximum E of the brain is the smaller than that of the skull and scalp. When no shielding ring is present in the horizontal direction of the WCC, the maximum E of the human trunk and head is greater than that with the copper shielding ring. With the addition of the copper shielding ring, the maximum E of the

Table 6. Comparison between the maximum value of the $B\,(\mu\mathrm{T})$ of human tissues under different shielding conditions and the ICNIRP public exposure reference limit.

$B\,(\mu\mathrm{T})$	WCC horizontal direction unshielded			WCC with copper shielding in horizontal direction		
	Simulation value	ICNIRP limit value	Simulation value/Limit value	Simulation value	ICNIRP limit value	Simulation value/Limit value
Trunk	2.31×10^{1}	2.70×10^{1}	8.56×10^{-1}	1.32×10^{1}	2.70×10^{1}	4.89×10^{-1}
Entire head	4.40×10^{-2}	2.70×10^{1}	1.62×10^{-3}	2.48×10^{-2}	2.70×10^{1}	9.18×10^{-4}
Scalp	4.40×10^{-2}	2.70×10^{1}	1.62×10^{-3}	2.48×10^{-2}	2.70×10^{1}	9.18×10^{-4}
Skull	4.22×10^{-2}	2.70×10^{1}	1.56×10^{-3}	2.38×10^{-2}	2.70×10^{1}	8.81×10^{-4}
Brain	4.11×10^{-2}	2.70×10^{1}	1.52×10^{-3}	2.32×10^{-2}	2.70×10^{1}	8.59×10^{-4}

Table 7. Comparison between the maximum value of the $E\,(\mathrm{V/m})$ of human tissues under different shielding conditions and the ICNIRP public exposure reference limit.

$E\,(\mathrm{V/m})$	WCC horizontal direction unshielded			WCC with copper shielding in horizontal direction		
	Simulation value	ICNIRP limit value	Simulation value/Limit value	Simulation value	ICNIRP limit value	Simulation value/Limit value
Trunk	2.63×10^{0}	1.15×10^{1}	2.28×10^{-1}	1.47×10^{0}	1.15×10^{1}	1.27×10^{-1}
Entire head	9.87×10^{-3}	1.15×10^{1}	8.58×10^{-4}	6.04×10^{-3}	1.15×10^{1}	5.25×10^{-4}
Scalp	6.22×10^{-3}	1.15×10^{1}	5.41×10^{-4}	3.81×10^{-3}	1.15×10^{1}	3.31×10^{-4}
Skull	9.87×10^{-3}	1.15×10^{1}	8.58×10^{-4}	6.04×10^{-3}	1.15×10^{1}	5.25×10^{-4}
Brain	1.0×10^{-3}	1.15×10^{1}	8.70×10^{-5}	5.95×10^{-4}	1.15×10^{1}	5.17×10^{-5}

human trunk and head are reduced at 5.6×10^{-1} times and 6.1×10^{-1} times that of the WCC without the shielding ring in the horizontal direction.

The maximum B and E of the human trunk without the shielding ring in the horizontal direction of the WCC are 8.56×10^{-1} times and 2.28×10^{-1} times of the ICNIRP exposure limit, respectively. After adding the copper shielding ring, the values are reduced to 4.89×10^{-1} times and 1.27×10^{-1} times. The maximum B and E of the human head without the shielding ring in the horizontal direction of the WCC are 1.62×10^{-3} times and 8.58×10^{-4} times of the ICNIRP exposure limit, respectively. After adding the copper shielding ring, the values are reduced to 9.18×10^{-4} and 5.25×10^{-4} times, thereby proving that the shielding effect of the WCC horizontal copper shielding ring is reliable.

4. CONCLUSION

In this study, a metal shielding ring at the transmitting end of the WCC is designed, and the influence of the metal shielding ring on the self inductance and mutual inductance of the coil is simulated and analyzed. The shielding effects of the metal shielding rings of different metals are also compared. By taking the MCR WCC of the EV as the electromagnetic exposure source, B and E of the pedestrian trunk tissue and the head CNS at the observation point outside the EV are simulated and calculated in the wireless charging of EV under different shielding conditions. Through simulation, calculation, and comparison, the following conclusions are drawn:

(1) Although the conductivity and permeability of aluminum, copper, and steel vary to some extent,

the horizontal shielding effect of the WCC is almost the same. However, copper is superior to the other two materials in terms of heat dissipation and corrosion resistance, so copper is chosen as the material for the new shielding ring.

(2) The maximum values of B and E of the human trunk appear at the toes. The maximum B of the human head appears in the scalp, and the maximum E appears in the skull. The maximum values of the B and E in the brain are both at minimum. After adding the new shield, the maximum B of the human trunk tissue is reduced by 43%; the maximum E is reduced by 44%; the maximum B of the human head is reduced by 44%; and the maximum E is reduced by 39%. The comparison results show that the new metal shielding ring designed in this work has good shielding effect on the electromagnetic exposure of the WCC of the EV.

(3) After adding the copper shielding ring, the maximum B and E of human trunk decreased from 8.56×10^{-1} times and 2.28×10^{-1} times of the ICNIRP exposure limit to 4.89×10^{-1} times and 1.27×10^{-1} times, respectively, and the maximum B and E of human head decreased from 1.62×10^{-3} times and 8.58×10^{-4} times of the ICNIRP exposure limit to 9.18×10^{-4} and 5.25×10^{-4} times, respectively. The maximum B and E values of the human trunk and head CNS are lower than the exposure limits specified by the ICNIRP. At this power level, the electromagnetic radiation of the human trunk and the head CNS meets the ICNIRP international electromagnetic radiation standard and provides a reference for the safety of pedestrians.

ACKNOWLEDGMENT

The authors acknowledge the financial support from the National Natural Science Fund of China (51567015) and (51867014).

Author Contributions:

Wenting Mou and Mai Lu conceived the research and contributed to the research survey and data analysis.

Conflicts of Interest:

The authors declare no conflict of interest.

REFERENCES

1. Ahmad, A., M. S. Alam, and R. Chabaan, "A comprehensive review of wireless charging technologies for electric vehicles," *IEEE Transactions on Transportation Electrification*, Vol. 4, No. 1, 38–63, 2017.
2. Li, S. and C. C. Mi, "Wireless power transfer for electric vehicle applications," *IEEE Journal of Emerging and Selected Topics in Power Electronics*, Vol. 3, No. 1, 4–17, 2015.
3. Zhang, X., P. Zhang, Q. Yang, Z. Yuan, and H. Su, "Magnetic shielding design and analysis for wireless charging coupler of electric vehicles based on finite element method," *Transactions of China Electrotechnical Society*, Vol. 31, No. 1, 71–79, 2016.
4. Campi, T., S. Cruciani, F. Maradei, and M. Feliziani, "Magnetic shielding design of wireless power transfer system," *2015 31st International Review of Progress in Applied Computational Electromagnetics (ACES)*, 1–2, Williamsburg, 2015.
5. Kim, J., H. Kim, C. Song, I.-M. Kim, Y.-I. Kim, and J. Kim, "Electromagnetic interference and radiation from wireless power transfer systems," *2014 IEEE International Symposium on Electromagnetic Compatibility (EMC)*, 171–176, Raleigh, 2014.
6. Zhang, X., Z. Wang, B. Wei, S. Wang, and Q. Yang, "Analysis of the influence of electric shield on space magnetic field in electric vehicle wireless charging system," *Transactions of China Electrotechnical Society*, Vol. 34, No. 8, 1580–1588, 2019.

7. Pavelek, M., M. Frivaldsky, and P. Spanik, "Influence of the passive shielding on the transfer characteristics of the wireless power transfer systems," *2017 19th International Conference on Electrical Drives and Power Electronics (EDPE)*, 94–99, Dubrovnik, 2017.
8. Lu, M. and K. D. T. Ngo, "Circuit models and fast optimization of litzshield for inductive-power-transfer coils," *IEEE Transactions on Power Electronics*, Vol. 34, No. 5, 4678–4688, 2019.
9. Lu, M. and K. D. T. Ngo, "Comparison of passive shields for coils in inductive power transfer," *IEEE Applied Power Electronics Conference and Exposition — APEC*, 1419–1424, 2017.
10. Park, S. W., "Evaluation of elecromagnetic exposure during 85 kHz wireless power transfer for electric vehicles," *IEEE Transactions on Magnetics*, Vol. 54, No. 1, 1–8, 2018.
11. Ding, P.-P., L. Bernard, L. Pichon, and A. Razek, "Evaluation of electromagnetic fields in human body exposed to wireless inductive charging system," *IEEE Transactions on Magnetics*, Vol. 20, No. 2, 1037–1040, 2014.
12. Shimamoto, T., I. Laakso, and A. Hirata, "In-situ electric field in human body model in different postures for wireless power transfer system in an electrical vehicle," *Physics in Medicine and Biology*, Vol. 60, No. 1, 163–173, 2015.
13. Shimamoto, T., I. Laakso, and A. Hirata, "Internal electric field in pregnant-woman model for wireless power transfer systems in electric vehicles," *Electronics Letters*, Vol. 51, No. 25, 2136–2137, 2015.
14. Shah, I. A., Y. Cho, and H. Yoo, "Safety evaluation of medical implants in the human body for a wireless power transfer system in an electric vehicle," *IEEE Transactions on Electromagnetic Compatibility*, Vol. 62, No. 2, 338–345, 2020.
15. De Santis, V., T. Campi, S. Cruciani, I. Laakso, and M. Feliziani, "Assessment of the induced electric fields in a carbon-fiber electrical vehicle equipped with a wireless power transfer system," *Energies*, Vol. 11, No. 3, 684, 2018.
16. Miwa, K., T. Takenaka, and A. Hirata, "Electromagnetic dosimetry and compliance for wireless power transfer systems in vehicles," *IEEE Transactions on Electromagnetic Compatibility*, Vol. 61, No. 6, 2024–2030, 2019.
17. Lan, J. and A. Hirata, "Effect of loudspeakers on the in situ electric field in a driver body model exposed to an electric vehicle wireless power transfer system," *Energies*, Vol. 13, No. 14, 3635, 2020.
18. SAE TIR J2954, Wireless Power Transfer for Light-Duty Plug-In/Electric Vehicles and Alignment Methodology; SAE International: Warrendale, PA, USA, 2016.
19. IEC 61980-1. Electric Vehicle Wireless Power Transfer (WPT) Systems-Part 1: General Requirements; International Electrotechnical Commission: Geneva, Switzerland, 2015.
20. Zhou, W., M. Lu, and B. Chen, "Safety evaluation on high frequency electromagnetic exposure in driver's cab of subway train," *China Railway Science*, Vol. 36, No. 5, 116–121, 2015.
21. Lu, M. and S. Ueno, "Comparison of the induced fields using different coil configurations during deep transcranial magnetic stimulation," *Plos One*, Vol. 12, No. 6, 1–12, 2017.
22. Lu, M. and S. Ueno, "Deep transcranial magnetic stimulation using figure-of-eight and halo coils," *IEEE Transactions on Magnetics*, Vol. 51, No. 11, 1–4, 2015.
23. Rush, S. and D. A. Driscoll, "Current distribution in the brain from surface electrodes," *Anesthesia and Analgesia*, Vol. 47, No. 6, 717723, 1968.
24. Gabriel, S., R. W. Lau, and C. Gabriel, "The dielectric properties of biological tissues: III. Parametric models for the dielectric spectrum of tissues," *Physics in Medicine and Biology*, Vol. 41, No. 11, 2271–2293, 1996.
25. Li, J. and M. Lu, "Safety evaluation on electromagnetic exposure of radio frequency antenna in typical subway platform," *China Railway Science*, Vol. 41, No. 2, 157–164, 2020.
26. Tian, R. and M. Lu, "Safety assessment of electromagnetic exposure in high-speed train carriage with full passengers," *Annals of Work Exposures and Health*, 1–14, 2020.
27. Başyiğit, I. B., A. Genç, and S. Helhel, "Effect of orientation of RF sources maintained within the enclosures on electrical shielding effectiveness performance," *Turkish Journal of Electrical Engineering and Computer Sciences*, Vol. 27, No. 4, 3088–3097, 2019.

28. Basyigit, I. B., H. Dogan, and S. Helhel, "The effect of aperture shape, angle of incidence and polarization on shielding effectiveness of metallic enclosures," *Journal of Microwave Power and Electromagnetic Energy*, Vol. 53, No. 2, 115–127, 2019.
29. Basyigit, I. B., and M. F. Caglar, "Investigation of the magnetic shielding parameters of rectangular enclosures with apertures at 0 to 3 GHz," *Electromagnetics*, Vol. 36, No. 7, 434446, 2016.
30. Zamanian, Z., S. M. J. Mortazavi, E. Asmand, and K. Nikeghbal, "Assessment of health consequences of steel industry welders' occupational exposure to ultraviolet radiation," *International Journal of Preventive Medicine*, Vol. 6, No. 1, 123, 2015.
31. ICNIRP, "Guidelines for limiting exposure to time-varying electric and magnetic fields (1 Hz to 100 kHz)," *Health Physics*, Vol. 99, No. 6, 818–836, 2010.
32. ICNIRP, "Guidelines for limiting exposure to electromagnetic fields (100 kHz to 300 GHz)," *Health Physics*, Vol. 118, No. 5, 483–524, 2020.